Structural behavior of continuous two-span prestressed concrete T beams with different tendon profiles

Uksun Kim, Ehab N. Ballu, Seongwon Hong, and Thomas H.-K. Kang

- An experimental program was conducted to investigate the behavior of indeterminate prestressed concrete T beams with two different unbonded tendon profiles. Three T beams, at half-scale size, were constructed for the test program. The control specimen had no eccentricity at the interior support, and the other specimens had eccentricity at the interior support.
- The experimental and theoretical results indicate that the specimens with eccentricity at the interior support had a greater number of cracks at the tension zone of the support than the control specimen. This finding was explained by hyperstatic moment reducing the negative moment in the control specimen.
- The authors conclude that the effect of hyperstatic moment should be accounted for in the calculation of concrete stress at the service level for continuous prestressed concrete beams with unbonded tendons and a vertically unconfined support condition.

Prestressed concrete members are categorized into two groups: bonded and unbonded. In a bonded member, the strand and concrete are assumed to behave as one body.[1,2] Equilibrium and local compatibility equations are then derived for design purposes. However, in an unbonded member, the concrete and tendon deform independently, so one must consider their global compatibility for any analytical purposes.[3,4] In other words, in the unbonded concrete member, the overall compression of the concrete is equal to the total tendon force along the location of the tendon. Therefore, any computational method to calculate the unbonded tendon stresses at various behavioral stages has become a point of interest for researchers and many have proposed methods of estimating the value of those stresses, as follows.

One of the common methods, load balancing, was proposed in 1972 by Lin and Thornton[3] to analyze prestressed concrete members. In 1990, Aalami[5] presented detailed concepts and procedures for load balancing with numerical analysis.

In 1993, Cohn and Lounis[7] presented research on an optimum limit design method for prestressed concrete structures. In 1997, Kodur and Campbell[8] evaluated and analyzed moment distribution in a two-span, continuous prestressed concrete beam, and Lopes et al.[9] investigated the degree of distribution in prestressed concrete beams by comparing their experimental data with the corresponding theoretical values.

In 2010, Nie et al.[12] presented an analytical and numerical model of prestressed, continuous steel-concrete composite beams and Zhou and Zheng[13] developed a plastic design method and formulated the degree of movement distribution for prestressed concrete beams with unbonded tendons by investigating experimental results.

In 2013, Lou et al.[14] analyzed the flexural behavior of continuous prestressed concrete beams using a finite-element model. In another paper published the next year, Lou et al.[15] analytically examined hyperstatic reactions and moment distribution of continuous concrete beams prestressed with external carbon-fiber-reinforced polymer tendons.

In two papers, coauthors Witchukreangkrai, Aravinthan, and Mutsuyoshi[16,17] proposed a method to enhance the flexural strength of beams that use the highly eccentric tendons. The primary moment given by the eccentricity of the prestressing caused the beam to camber upward at the interior supports, but restraints at the interior support prevented the upward deflection, which created a hyperstatic moment. This phenomenon resulted in reactions that were different from the reactions of a similar beam that had no applied prestressing.

In general, hyperstatic moment occurs when a pin or roller condition of a two-span prestressed concrete beam is used at the interior support. There have been few investigations, however, of hyperstatic action and mechanism in indeterminate prestressed concrete beams with unconfined interior conditions.[4] Furthermore, despite the frequent use of a T-shaped section in lieu of a rectangular section, most experimental research on continuous prestressed concrete beams has focused on the behavior of the rectangular section. The center of gravity of concrete is much closer to the top flange of T beams so that tendons are mostly located below the center of gravity of concrete.

In the research described in this paper, a series of experiments was conducted using two-span, prestressed high-strength concrete T beams with two different unbonded tendon profiles. The experiments were done to observe the structural behavior of the beams that were stressed by the prestressing strand as well as the resulting crack patterns under the same loading condition. Two seven-wire strands with a draped tendon profile were provided for each beam. The test program analyzed a case where tendon eccentricity was present at the interior support and a case where it was not. The two vertical point loads were applied to both spans simultaneously. Deflection and stress at the prestressing reinforcement were then measured. Based on the support reaction, the hyperstatic moment at the interior support was analyzed, which was in an unconfined condition.

Experimental program

Design of test specimens

The test program included experiments on three approximately half-scale specimens to understand the overall behavior of indeterminate prestressed concrete T beams with two different unbonded tendon profiles.

T beam specimen 1 (TB1) was designed with a double-harped tendon with no eccentricity at the interior support (**Fig. 1**). T beam specimens 2a and 2b (TB2a and TB2b) had the same tendon profile, but the eccentricity δ_1 was 2.7 in. (68.6 mm) at the interior support (**Fig. 2**). TB1 was a control specimen without any eccentricity at the interior support, whereas TB2a and TB2b were designed to have eccentricity at the interior support.

Figures 1 and 2 show the dimensions and reinforcement details for the three specimens. All specimens were 360 in. (9144 mm) long and 10 in. (254 mm) deep (including 2.5 in. [63.5 mm] of slab depth); the specimens were 13.5 in. (343 mm) wide at the top and 6.5 in. (165 mm) wide at the bottom web. High-strength concrete with compressive strength f'_c of 7.25 ksi (50 MPa) was used to construct all three beams.

To construct each specimen, four 240 in. (6096 mm) long, ASTM A615[18] Grade 60 (414 MPa) no. 3 (10M) bars with a yield strength of bonded reinforcement F_y of 60 ksi (420 MPa) were placed on sawhorses in pairs. Given the concrete cover at both ends, the total length for each pair was 358 in. (9093.2 mm). (These reinforcing bars are shown as four no. 3 at interior support in Fig. 1 and 2). To provide greater flexural strength to the beams, one 120 in. (3048 mm) long, Grade 60 no. 3 bar was located in each pair. (This reinforcing bar is shown as one no. 3 in Fig. 1 and 2). Sixty-one 8 × 4.5 in. (203.2 × 114.3 mm) Grade 60 no. 3 stirrups were inserted and spaced 6 in. (152.4 mm) on center. Twelve 11.5 in. (292.1 mm) long, Grade 60 no. 3 bars were laid and centered perpendicularly at every 30 in. (762 mm) along the rectangular cage. The unbonded tendons were designed with double-harped profiles for all spans. The ¼ in. (6.35 mm) diameter, Grade 250 (1725 MPa) seven-wire strand with an ultimate tensile strength of bonded reinforcement F_u of 250 ksi (1750 MPa) was cut to 408 in. (10,363.2 mm), cleaned to remove surface rust, and then coated lightly with grease to facilitate insertion of the strand into the vinyl tube and reduce the friction losses between the strand and the vinyl. After placing the strand in the vinyl tube, the tendon was inserted inside the cage according to the tendon profile.

Two tendon profiles were used for the three specimens. For TB1, the control specimen, a tendon end was placed at the centroid (located at the center of gravity of concrete) of the specimen and then the tendon profile was slightly inclined until it reached a distance of 71 in. (1803 mm) beyond the first (left) end of the beam. From that point, the tendon was extended horizontally for 38 in. (965 mm) (Fig. 1).

The same procedure was repeated for the next span. The tendon profile of two specimens (TB2a and TB2b) was the same, except that it was located 2.7 in. (68.6 mm) above the

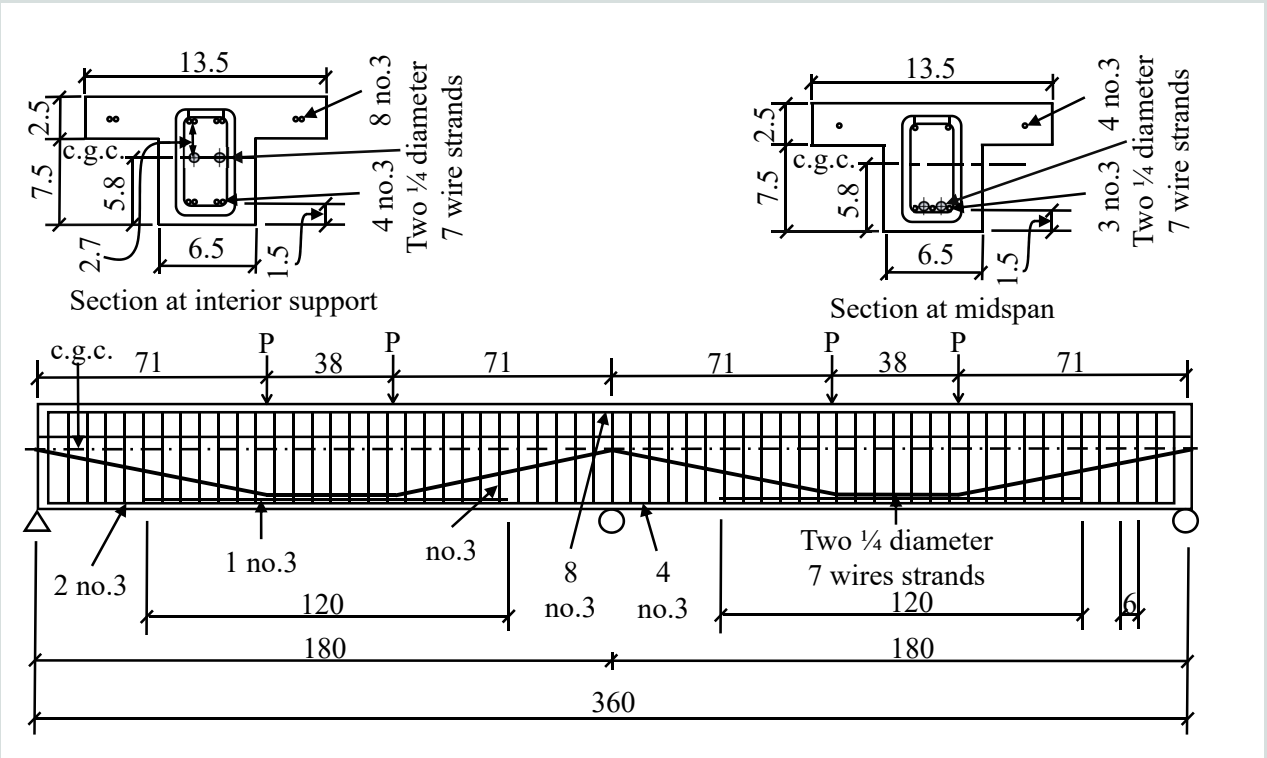

Figure 1. Dimensions and reinforcement details for the control specimen (TB1). Note: Units are in inches. c.g.c. = center of gravity of concrete; *P* = vertical load. No. 3 = 10M; 1 in. = 25.4 mm.

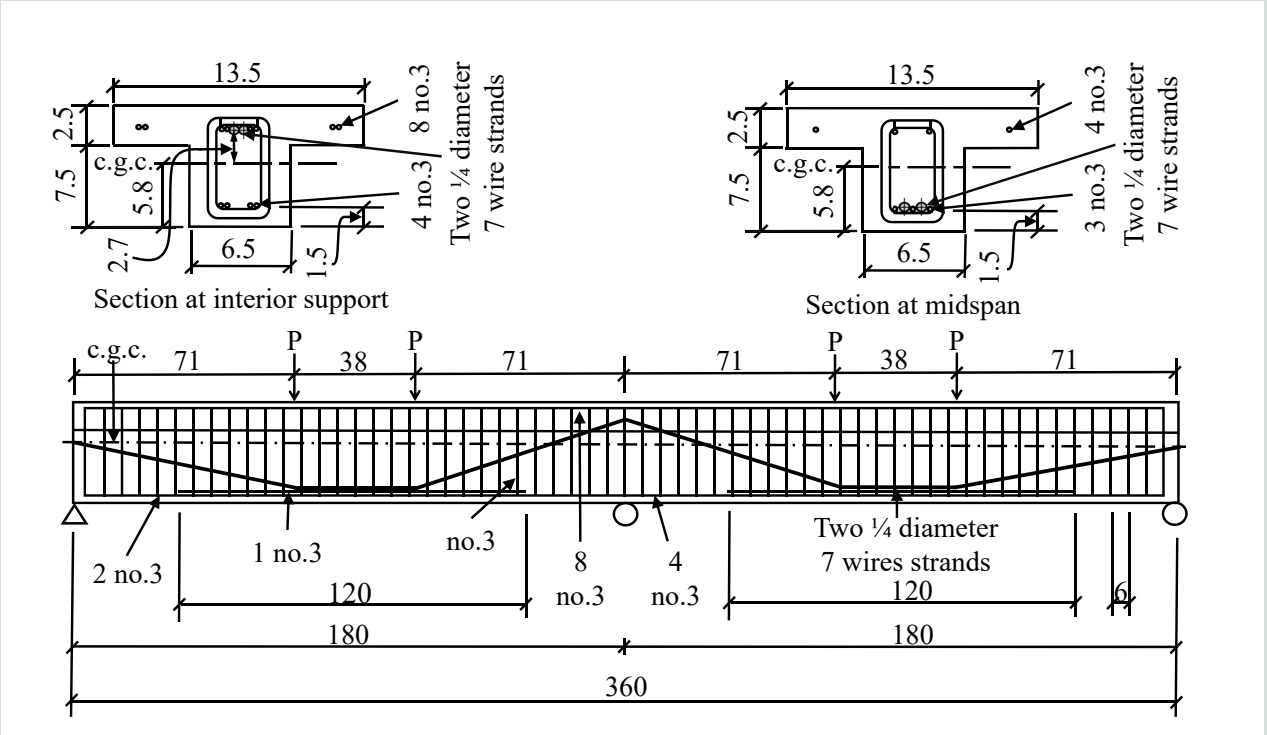

Figure 2. Dimensions and details of reinforcement of T beam specimens 2a and 2b (TB2a and TB2b). Note: Units are in inches. c.g.c. = center of gravity of concrete; *P* = vertical load. No. 3 = 10M; 1 in. = 25.4 mm.

centroid of the T beam at the interior support, allowing 1.5 in. (38.1 mm) of concrete cover from the top (Fig. 2).

Twelve strain gauges were placed on the reinforcing bars of each beam (**Fig. 3**). Six strain gauges (SG1, SG2, SG3, SG9, SG10, and SG11) were installed on the reinforcing bars in each span, where maximum positive moment at each span was expected, with a gauge length of 8 in. (203.2 mm). Three strain gauges (SG5, SG6, and SG7) were placed on the reinforcing bars at the interior support, which yielded maximum negative bending moment. SG5 and SG7 were positioned 8 in. (203 mm) from SG6. SG4 and SG8 were placed on reinforcing bars at the bottom of the beam, where the second point load would be applied, to measure the tension stress, and SG12 was located on a reinforcing bar at the bottom of the interior support to measure the compression stress at that point.

Loading and measurement

After the beam was placed in the loading frame (**Fig. 4**), the 12 strain gauges were connected to the data acquisition system. A special load cell frame was designed and fabricated to house the load cells at the supports. All three supports—one each at the two ends and one in the interior—had the same support condition, which was a steel roller (Fig. 4). To observe the actual deflection under a given loading, two linear variable displacement transducers (LVDTs) were placed under the beam where the maximum theoretical deflection would occur. All LVDT wires were attached to the bottom of the specimen at the north and south spans. All load cells and LVDTs were connected to the dual display multimeters, load cell indicators, and data acquisition system.

An electric hydraulic jack was used to stress the strands up to 70% of the specified tensile strength of prestressing steel $0.7f_{pu}$ (189 or 6.8 kip [1.3 or 30.2 kN]) after seating loss. To achieve the initial stress of $0.7f_{pu}$, the prestressing load was incrementally applied at 900, 3500, and 7000 lb (4, 15.6, and 31.1 kN) (jacking load per each strand). At each increment, the prestressing process was stopped while readings from the load cells were recorded manually. The readings included prestressing force in both strands, deflection in the north and south spans, reactions, and strand elongation. In addition, the jack pressure data from the hydraulic jack dial were documented. Steel plates measuring 6 × 6 × 0.5 in. (152.4 × 152.4 × 12.7 mm) were placed between the specimen and load cell. Because of the narrow web width, there was an interference problem between the east and west load cells, so a circular hollow bar was inserted between the load cells and the steel plate (Fig. 4).

After the strands were tensioned, the jack was released and the tendon force was maintained by the chucks; then the beam was ready to be loaded vertically. Two actuators (55 kip [244.7 kN] capacity) were used to apply the vertical load to both spans simultaneously as a two-point load. The data were

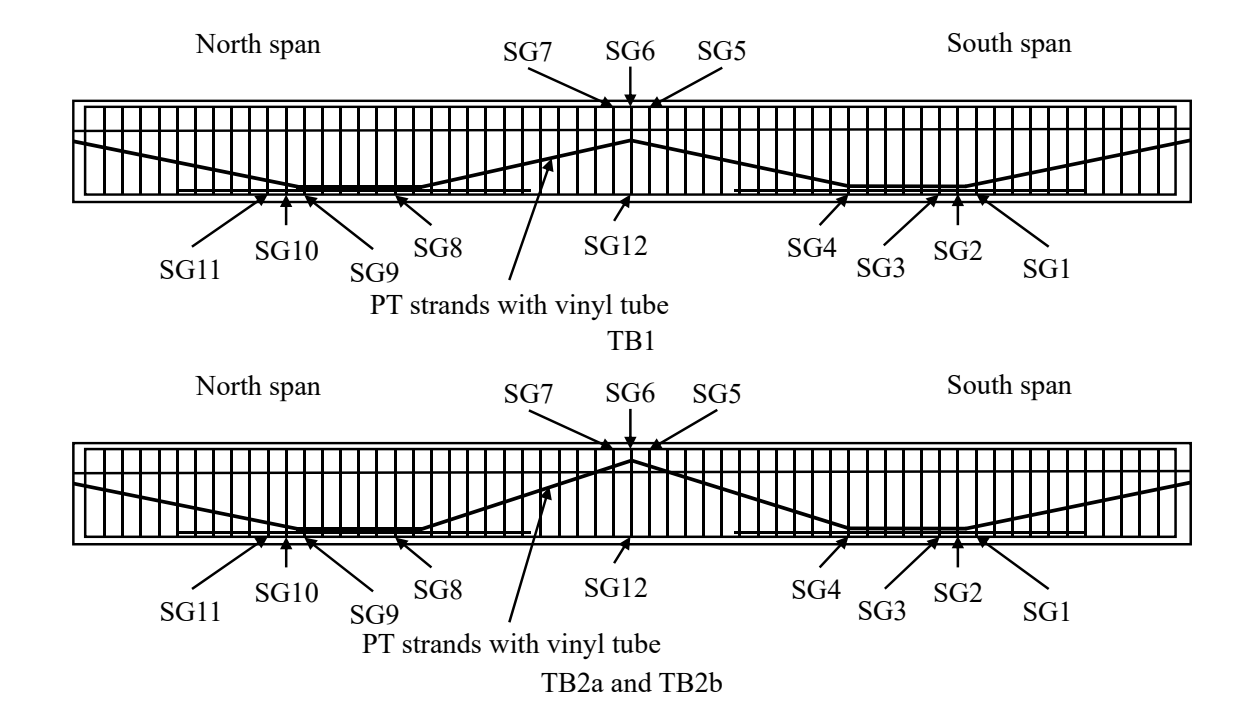

Figure 3. Location of strain gauges placed on longitudinal reinforcing bars. Note: PT = post-tensioned; SG1 = strain gauge 1; SG2 = strain gauge 2; SG3 = strain gauge 3; SG4 = strain gauge 4; SG5 = strain gauge 5; SG6 = strain gauge 6; SG7 = strain gauge 7; SG8 = strain gauge 8; SG9 = strain gauge 9; SG10 = strain gauge 10; SG11 = strain gauge 11; SG12 = strain gauge 12; TB1 = T beam specimen 1; TB2a = T beam specimen 2a; TB2b = T beam specimen 2b.

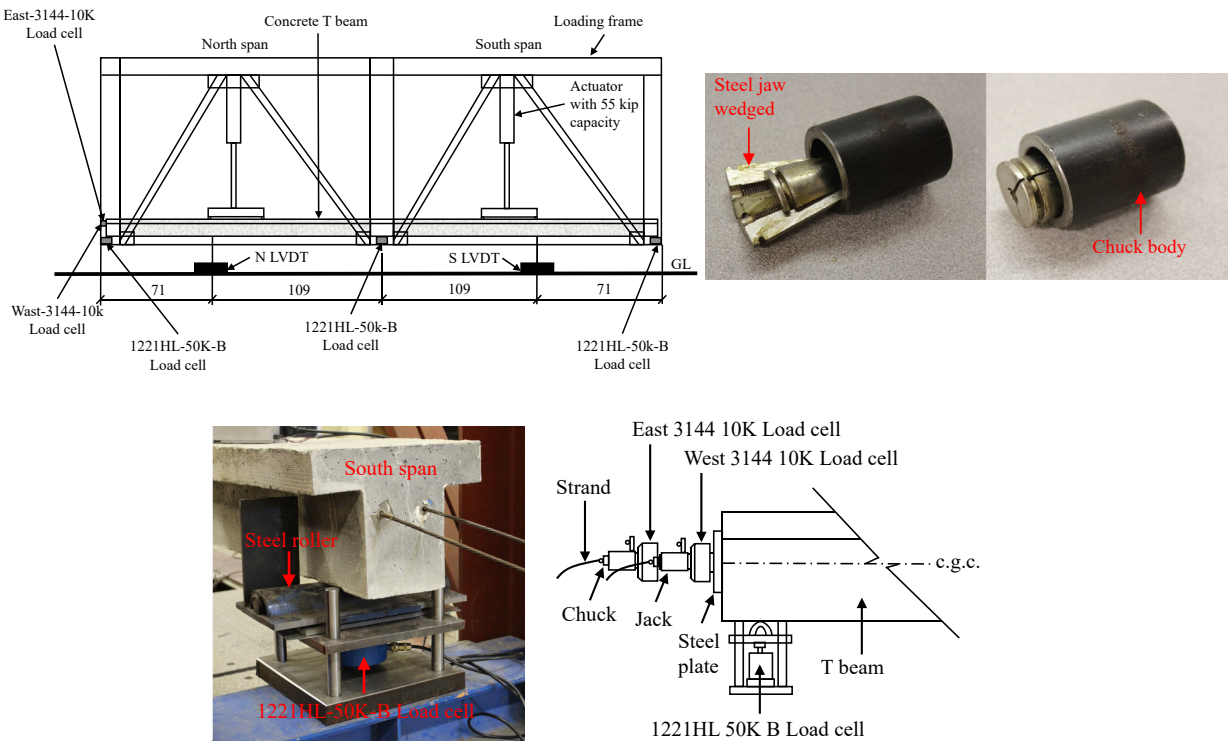

Figure 4. Loading frame, load cell details, linear variable displacement transducers (LVDTs), steel jaw, and chuck. Note: Units are in inches. c.g.c. = center of gravity of concrete; NLVDT = north-span linear variable displacement transducer; SLVDT = south-span linear variable displacement transducer. 1 in. = 25.4 mm; 1 kip = 4.448 kN.

recorded in increments of 1 second. The loading process was stopped at every 1 kip (4.448 kN) increment to record the tendon force and reaction data. The loading was stopped when the stress applied to the strand reached $0.7f_{pu}$.

Crack propagation patterns were also recorded manually throughout the test. The first cracking load was recorded. After each additional loading, new cracks developed, and these were traced and labeled with a number at the top of the crack. All cracking loads were recorded at their corresponding locations. The same procedure was conducted for all three specimens.

Test results

Responses of deflection versus load curve

Figure 5 presents for each specimen the total deflection

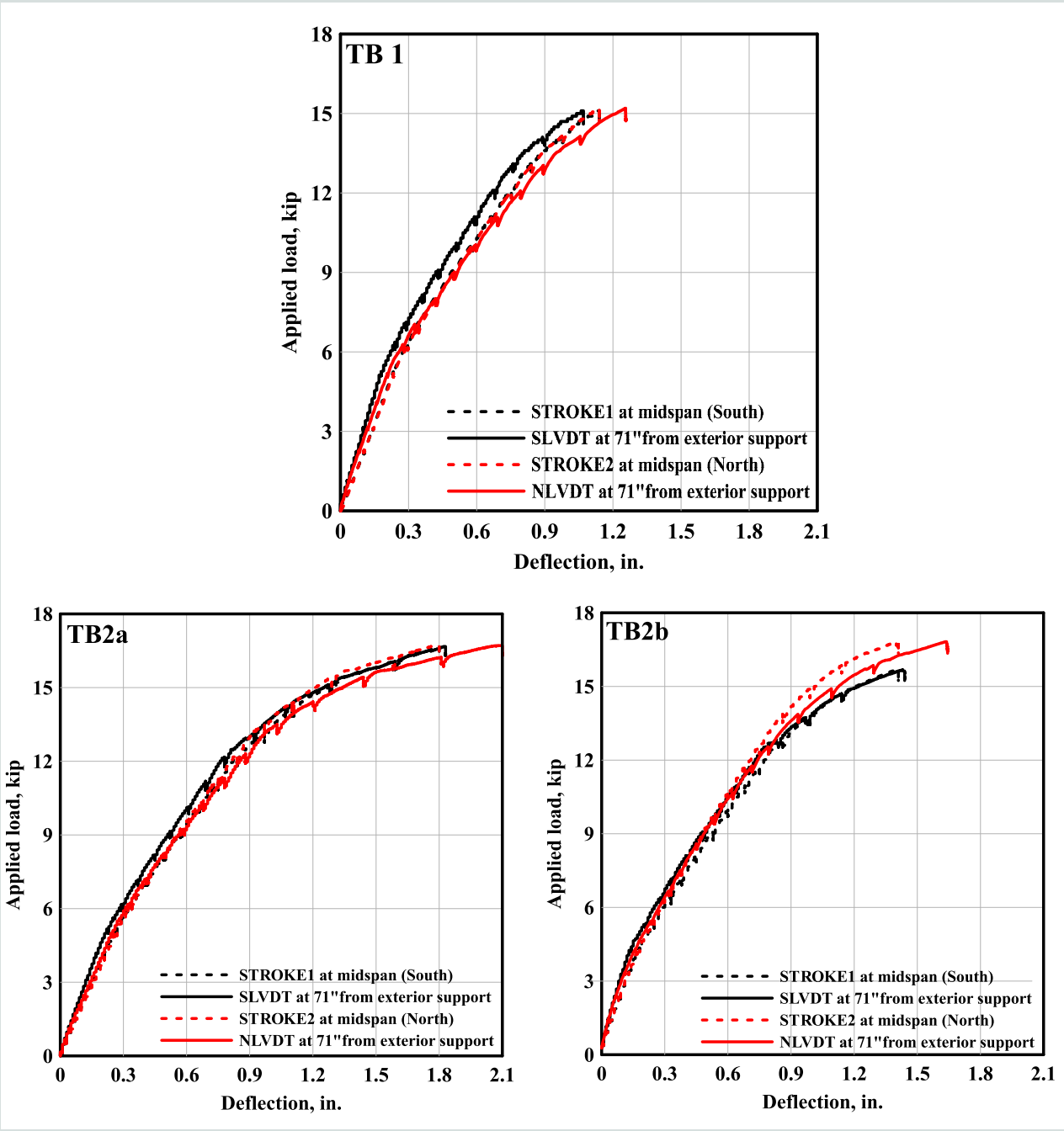

Figure 5. Deflection versus applied load curve. Note: NLVDT = north-span linear variable displacement transducer; SLVDT = south-span linear variable displacement transducer; STROKE1 = linear actuator stroke at midspan (south); STROKE2 = linear actuator stroke at midspan (north); TB1 = T beam specimen 1; TB2a = T beam specimen 2a; TB2b = T beam specimen 2b. 1" = 1 in. = 25.4 mm; 1 kip = 4.448 kN.

versus applied load curves at two locations: midspan and 71 in. (1803 mm) from the exterior supports. The deflections were measured at the locations of the two LVDTs and the strokes (at the actuators), and the tests were stopped before the beam failed. In the cases of TB1 and TB2a, the north span exhibited greater deflection than the south span when subjected to the same applied load, whereas the deflection at the south span was greater than at the north span for TB2b. This asymmetric behavior indicates that the tendon behavior might be asymmetrical. The reason why deflection of the north span in TB2b was lower than that of the south span might be that the south span had a fixed end of tendons, even though the tendon profiles of TB2b were installed symmetrically. The differences between the deflections recorded from the LVDTs and the strokes can be attributed to the fact that continuity in the two-span beams shifted the maximum deflection position

from the midspan toward the exterior supports where the load at the first harp was applied.

The prestressing tendon profile did not have a significant effect on the initial stiffness of the specimens for the following reasons:

- The concrete stress produced by the prestressing balanced some of the stress of the applied load and correspondingly reduced the deflection, resulting in essentially no cracking for the specimens.
- The initial stiffness, which is mostly based on the sectional properties of the structural member, was the same for all specimens.

Even though testing of the beams was stopped before their ultimate limit state was reached, the larger measured load for TB1 than for TB2a and TB2b at the same deflection signals that the larger load capacity is anticipated due to the larger negative moment capacity at the beam section near the interior support.

Behavior of bonded reinforcing bars

Figure 6 shows relationships for the three specimens between the applied load and strain on bonded longitudinal reinforcing bars. The detailed locations of strain gauges were illustrated in Fig. 3. The reinforcing bar strains of TB1 and TB2b at SG1, located at the starting point of the first harp at the south span, were 2832 and 2492 με, respectively, under the applied load of 14.7 kip (65.4 kN). For TB2a, the reinforcing bar yielded at a load of 14.8 kip (65.8 kN) and a maximum strain of 2291 με, which yielded perfectly plastic deformation. At the SG3 position, the yielding point of the reinforcing bar in TB1 and TB2b was detected at approximately 14 kip (62.3 kN) with a strain of 2820 με, whereas the reinforcing bar in TB2a yielded at the higher load (approximately

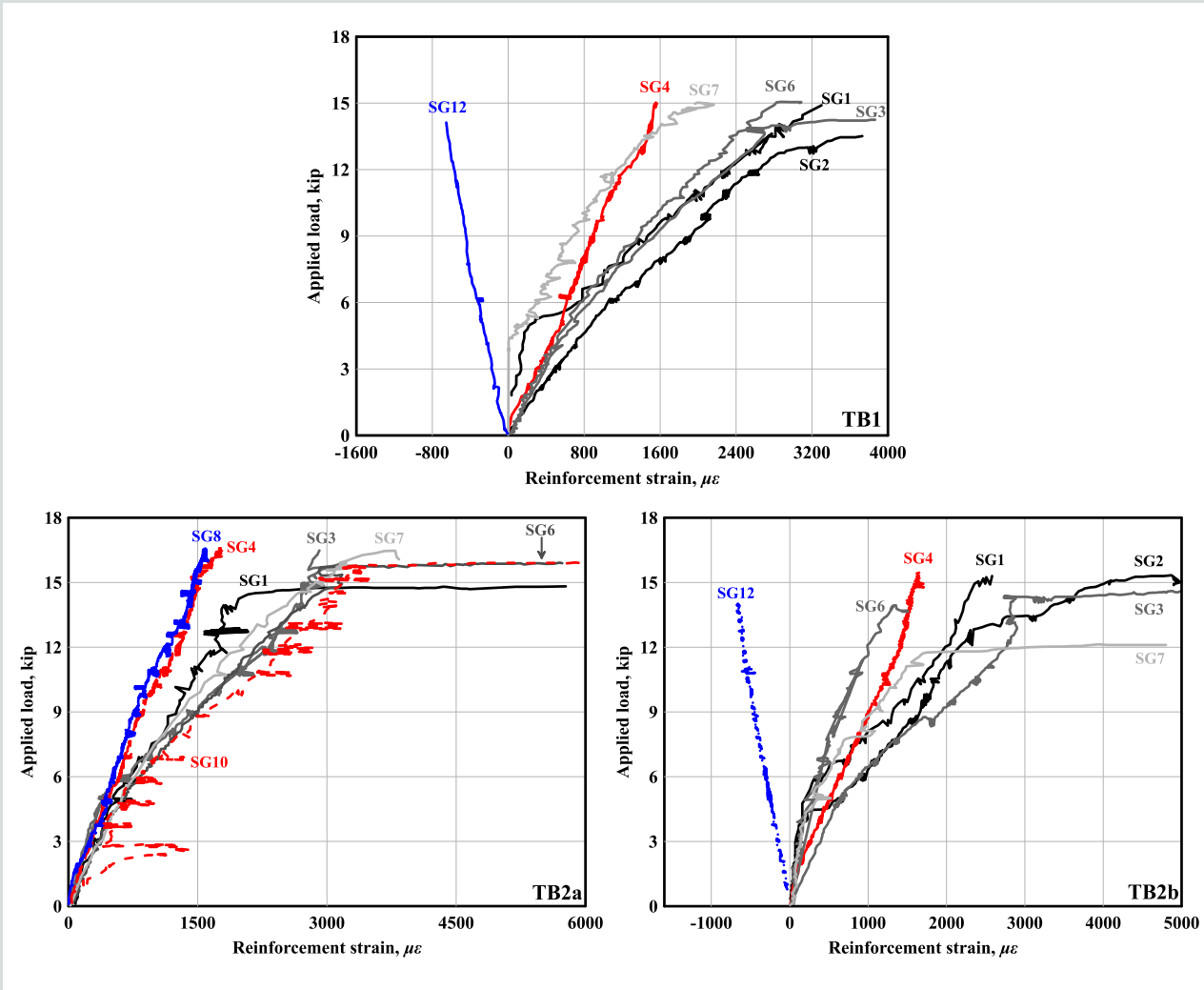

Figure 6. Reinforcement strain results. Note: SG1 = strain gauge 1; SG2 = strain gauge 2; SG3 = strain gauge 3; SG4 = strain gauge 4; SG6 = strain gauge 6; SG7 = strain gauge 7; SG8 = strain gauge 8; SG10 = strain gauge 10; SG12 = strain gauge 12; TB1 = T beam specimen 1; TB2a = T beam specimen 2a; TB2b = T beam specimen 2b. 1 kip = 4.448 kN.

16.5 kip [63.4 kN]). In TB1 and TB2b, the reinforcing bar strain deformation curves at SG4, placed at the second harp point of the south span, were almost identical to each other and did not reach steel yielding. Strain gauges SG6 and SG7 were installed at the interior support at the tension zone. At the location of SG6, the reinforcing bar in TB1 yielded at a load of 15.1 kip (67.2 kN) and the maximum strain was 2883 με. The strain slopes of TB1 and TB2a recorded by SG7 were almost identical to one another: reinforcement in TB1 and TB2a yielded at loads of 13.5 and 13.2 kip (60.1 and 58.7 kN), respectively, and the maximum strains were 2318 and 2354 με, respectively.

SG12 was placed exactly at the interior support in the compression zone. Despite the fluctuation in some of the data, the slopes of the lines were close to each other. The applied load and reinforcing bar strain for TB1 were 14.5 kip (64.5 kN) and -674 με, respectively. For TB2b, they were 13.7 kip (60.9 kN) and -667 με, respectively. The steel bars at the interior support yielded first. Strain gauge data for TB2a were not available.

For all specimens, all of the nonprestressed steel bars at the point where the first load was applied yielded at a comparable loading state. This behavior can be due to the maximum positive moment occurring at the first point load from external support for the north and south spans and the maximum negative moment occurring at the interior support. In both spans, the steel bars at the second point load did not yield. The steel bars at the bottom of the interior support did not reach the compressive yielding point, and as a result, the prestressing had no noticeable effect at the compression zone of the interior support. The primary moment due to prestressing deflected the beam—including at the interior support—upward, which caused an increase in the compression stress at the bottom fiber of the beam at that location, where no cracks developed on either the top or bottom surfaces.

Stress at prestressing reinforcement

The stress in the unbonded prestressing reinforcement f_{ps} at nominal flexural strength can be calculated by the method set forth in section 20.3.2.4.1 of the American Concrete Institute's *Building Code Requirements for Structural Concrete (ACI 318-19) and Commentary (ACI 318R-19)*,[19] as shown in **Table 1**.

Determining the stress in the prestressing strand was complicated because of the many variables and parameters. In addition, because the test was stopped before failure, the final point was not the stress in the unbonded prestressing steel at nominal flexural strength. The decision to stop before failure was due to safety issues and because the allowable deflection limit had been exceeded. Because the distance from the extreme compression fiber to the centroid of reinforcement steel at the interior support was different for TB1 and TB2a, the slopes of the applied load–strand tension relationship were also different for the two specimens (**Fig. 7**). Specifically, the slope of the applied load–strand tension relationship for TB2a, which had a larger tendon profile depth, was greater than the slope for TB1. The first cracking in TB2a and TB2b occurred at a lower applied load than the first cracking in TB1; however, the unbonded tendons of TB2a and TB2b seemed to take over the larger external load after cracking. The data from a load cell in TB2b were almost the same as those from TB1 up to 14 kip (62.3 MPa), after which monitoring was stopped. The other load cell of TB2b malfunctioned and could not be read from the beginning.

Table 1. Specified stress in unbonded prestressing reinforcement f_{ps} at nominal flexural strength for unbonded tendons

$\frac{l_n}{h}$	f_{ps}, ksi	
≤35	The least of	$f_{se} + 60{,}000 + \frac{f'_c}{(100\rho_p)}$
		$f_{se} + 60{,}000$
		f_{py}
>35	The least of	$f_{se} + 10{,}000 + \frac{f'_c}{(300\rho_p)}$
		$f_{se} + 30{,}000$
		f_{py}

Source: Equation from American Concrete Institute (ACI) 318-19 section 20.3.2.4.1.

Note: A_{ps} = area of prestressing longitudinal tension reinforcement; b = width of compression face of member; d_p = distance from extreme compression fiber to centroid of prestressing reinforcement; f'_c = specified compressive strength of concrete; f_{py} = specified yield strength of prestressing reinforcement; f_{se} = effective prestress; h = height of member; l_n = length of clear span measured from face to face of supports; ρ_p = ratio of A_{ps} to bd_p. 1 ksi = 6.985 MPa.

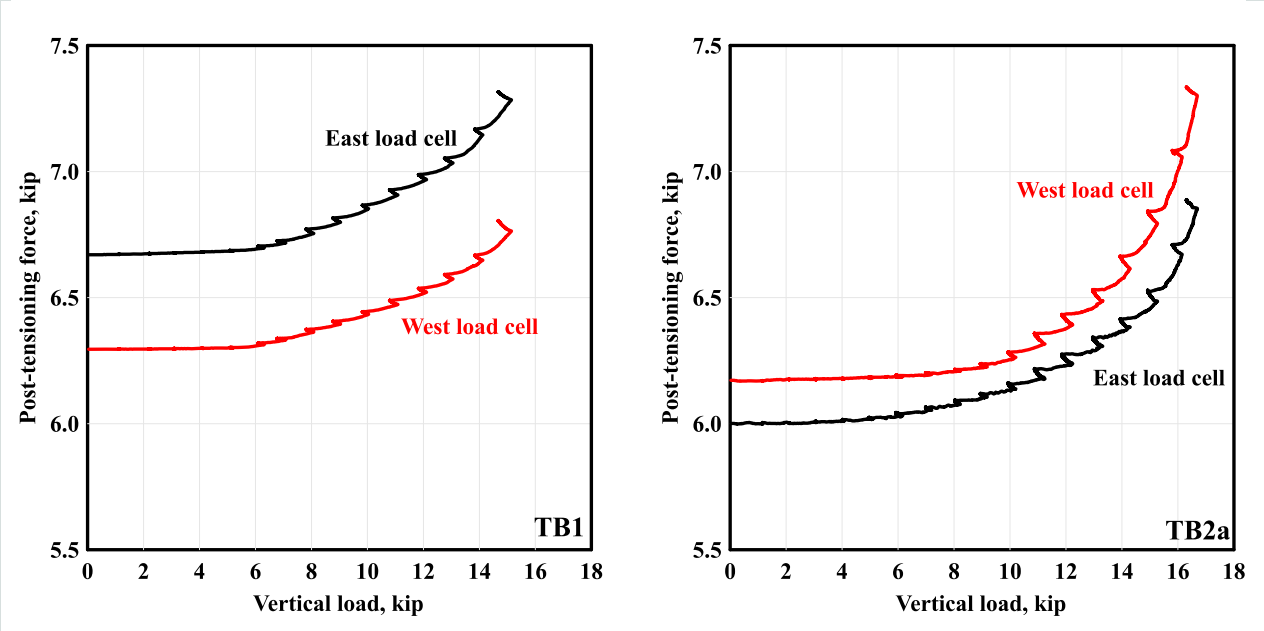

Figure 7. Applied load–strand tension relationships for specimens TB1 and TB2a Note: TB1 = T beam specimen 1; TB2a = T beam specimen 2a. 1 kip = 4.448 kN.

Figure 8. Crack patterns for T beam specimen 1 (TB1).

Figure 9. Crack patterns for T beam specimen 2a (TB2a).

Crack distribution and propagation

Figures 8 and **9** show that cracks in TB1 and TB2a occurred first at the tension face (top) of the interior support and then cracking started at the tension face (bottom) at the midspan in both the north and south spans. The cracks in the interior supports distributed uniformly from both sides, but there were fewer cracks in TB1 than in TB2a and TB2b. The reason for the differences in the two TB2 specimens' behavior was the positive hyperstatic moment induced in the supports. This moment was greater for TB1 than for TB2a and TB2b and, as a result, there was a greater reduction of negative moment in TB1. On the other hand, the distribution of the cracks at the north and south spans ranged from the first point load applied, which was 71 in. (1803.4 mm) from the external support in both spans, to the midspan of each span. This behavior was due to the maximum positive moment occurring at that location.

Investigation of hyperstatic actions

Direct method

In general, hyperstatic moments of continuous indeterminate structure are determined through the direct method (also called load-balancing method).[5] Although the interior supports were not pin or roller connected, hyperstatic moment and reaction at the initial stages were calculated and compared with the experimental data. The direct method procedure was initiated by prestressing strands that were converted into corresponding equivalent loading and applied to the concrete. **Figure 10** shows the equivalent loading due to the prestressing tendon profile in the concrete of TB1 with its corresponding primary, hyperstatic, and combined moments. Note that unlike hyperstatic moment (actual beam internal moment due to external reaction), primary moment is not an actual internal moment of the beam but is an assumed effect on concrete only when tendons are replaced by equivalent load. In real-life scenarios, beams would be seated on top of the interior support and vertical upward restraint would not exist. For this reason, the procedure was also applied with no interior support reaction to account for zero hyperstatic moment (**Tables 2** and **3**). **Figure 11** displays the equivalent loading due to prestressing tendon profile in the concrete of TB2a and TB2b with its corresponding primary, hyperstatic, and combined moments.

Comparison of theoretical and experimental results

Theoretical results were first compared based on the roller support condition with vertical restraint with the experimental

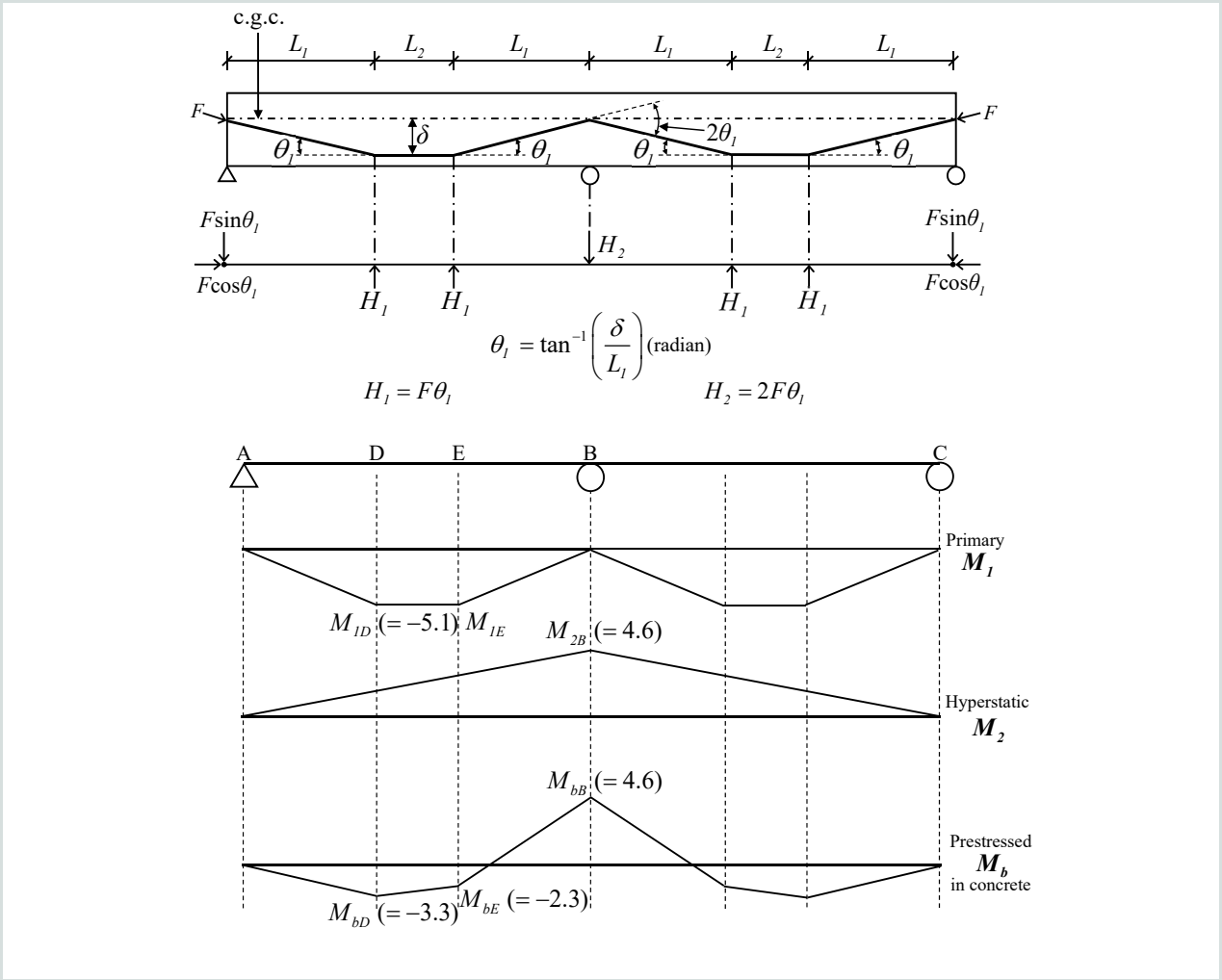

Figure 10. Equivalent load to concrete beam and corresponding moment diagrams primary, hyperstatic, and combined moments in concrete of T beam specimen 1 (TB1). Note: Units are in kip-ft. F = prestressing force; H_1 = equivalent concentrated load calculated by θ_1; H_2 = equivalent concentrated load calculated by $2\theta_1$; L_1 = distance between the end support and the concentrated loading point; L_2 = distance between two concentrated loading points; M_b = combined moment; M_{bB} = combined moment at point B; M_{bD} = combined moment at point D; M_{bE} = combined moment at point E; M_1 = primary moment; M_{1D} = primary moment at point D; M_2 = hyperstatic moment; M_{2B} = hyperstatic moment at point B; δ = distance between the line of prestressing force and the lowest sag point of tendon profile; θ_1 = angle of the profile at H1; θ_2 = angle of the profile at H_2. 1 kip-ft = 1.356 kN-m.

Table 2. Comparison of theoretical and experimental changes at the interior support immediately after transfer

Specimen	Theoretical hyperstatic moment, kip-ft	Theoretical reaction reduction,* lb		Experimental reaction reduction, lb	Experimental reaction reduction/theoretical reaction reduction, %	
		With vertical restraint	Without vertical restraint		With vertical restraint	Without vertical restraint
TB1	4.63	617	0	546	88.4	Infinite
TB2a	2.91	388	0	282	72.7	Infinite
TB2b	2.91	388	0	365	94.1	Infinite

Note: TB1 = T beam specimen 1; TB2a = T beam specimen 2a; TB2b = T beam specimen 2b. 1 lb = 4.448 N; 1 kip-ft = 1.356 kN-m.

Table 3. Comparison of theoretical and experimental changes at the interior support after 24 hours

Specimen	Theoretical hyperstatic moment, kip-ft	Theoretical reaction reduction, lb		Experimental reaction reduction, lb	Experimental reaction reduction/theoretical reaction reduction, %	
		With vertical restraint	Without vertical restraint		With vertical restraint	Without vertical restraint
TB1	4.63	617	0	549	88.9	Infinite
TB2a	2.91	388	0	311	80.2	Infinite
TB2b	2.91	388	0	241	62.1	Infinite

Note: TB1 = T beam specimen 1; TB2a = T beam specimen 2a; TB2b = T beam specimen 2b. 1 lb = 4.448 N; 1 kip-ft = 1.356 kN-m.

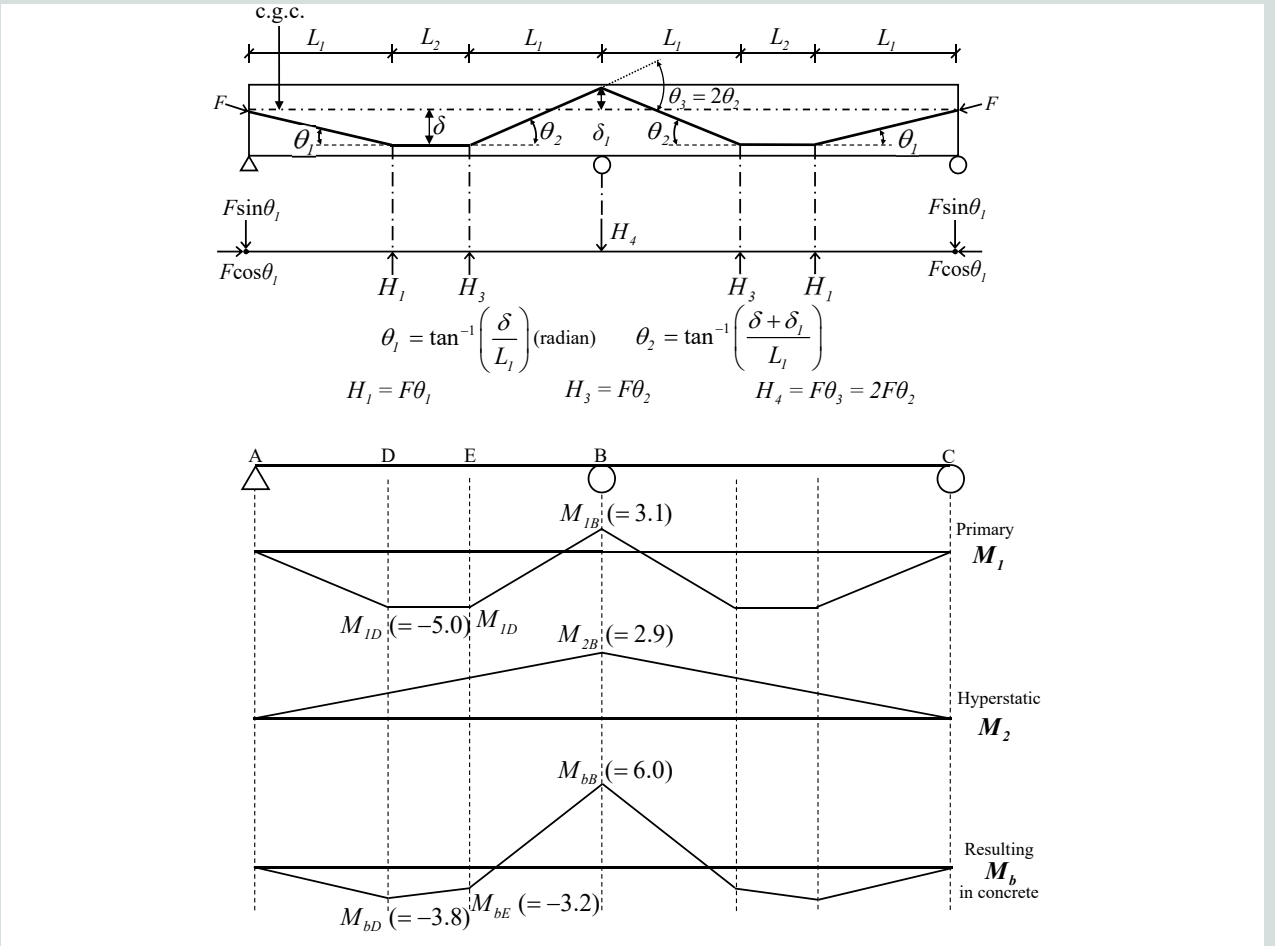

Figure 11. Equivalent load to concrete and corresponding moment diagrams for primary, hyperstatic, and combined moments in concrete of T beam specimens 2a and 2b (TB2a and TB2b). Note: Units are in kip-ft. F = prestressing force; H_1 = equivalent concentrated load calculated by θ_1; H_3 = equivalent concentrated load calculated by θ_2; H_4 = equivalent concentrated load calculated by θ_3; L_1 = distance between the end support and the concentrated loading point; L_2 = distance between two concentrated loading points; M_b = combined moment; M_{bB} = combined moment at point B; M_{bD} = combined moment at point D; M_{bE} = combined moment at point E; M_1 = primary moment; M_{1B} = primary moment at point B; M_{1D} = primary moment at point D; M_2 = hyperstatic moment; M_{2B} = hyperstatic moment at point B; δ = distance between the line of prestressing force and the lowest sag point of tendon profile; δ_1 = distance between the line of prestressing force and the highest point of tendon profile at center; θ_1 = angle of the profile at H_1; θ_2 = angle of the profile at H_3; θ_3 = angle of the profile at H_4. 1 kip-ft = 1.356 kN-m.

results. Tables 2 and 3 compare the theoretical[5] and experimental reaction values at the interior support before the external loading was applied. The theoretical reaction is simply determined from hyperstatic moment, with and without vertical restraint. The experimental data recorded for TB1 show the closest correspondence to the theoretical calculations (88.4% and 88.9% at the time of stressing and after 24 hours, respectively). Unlike TB1, TB2a and TB2b had eccentricity at the interior support, which might have caused the strand to take more time to redistribute the internal forces. Cold welding (or contact welding) was considered the primary reason why hyperstatic moment at the interior support occurred. Even though the interior support was not restrained, the self-weight of the beam worked as a restraint so that the interior support of the beam became a partial roller condition. The primary moment caused the beam at the interior support to deflect upward, but the hyperstatic moment tried to reduce that upward movement. Once the hyperstatic moment occurred at the interior support, the hyperstatic moment value could be interpolated at any other point along the span of the T beam.

Figure 12 shows reaction-deflection curves for all three specimens. As mentioned earlier, the deflection was measured at a horizontal distance of 71 in. (1803 mm) from the exterior supports and the average value of two deflections was used for plotting the reaction-deflection curve at the interior support. In Fig. 12, the black solid lines represent the reaction at each support—interior support, south support, and north support—and the black dashed lines were calculated from the total applied load multiplied by the proportion 4.23/6.23, which is obtained from elastic analysis of an indeterminate beam and expected to be the same until plastic moment is reached. The gray dashed lines show the differences between the experimental reactions and the portions of measured total actuator. As the external loading increased, the differences decreased and approached zero, signifying that hyperstatic reaction decreased at the interior support. In addition, the differences also decreased at the south and north support for all three specimens. There was hyperstatic reaction due to cold welding effect immediately before the external loading; hyperstatic reaction then decreased as the loading increased and eventually approached zero, which indicates that the cold welding effect disappeared. The reason may be that cracking occurred at the interior support and the hyperstatic moment tended to be almost constant because the restrained relative rotation no longer existed at the interior support.

Kim and Kang[4] reported that the hyperstatic moment increased dramatically as the external load was increased for unbonded post-tensioned beams with three to five draped tendons per continuous beam; however, additional experimental research is warranted to confirm this finding. Unconfined interior support condition is common for continuous prestressed concrete beams in bridge structures, and ACI 318-19[19] requires inclusion of the values of concrete stress (at the service level) and moment demand (at the ultimate level) due to hyperstatic actions in the structural design.

Conclusion

Approximately half-scale tests were carried out to analyze and evaluate the structural performance of indeterminate prestressed concrete T beams with distinctive tendon profiles. The following conclusions were reached based on the investigation and comparison of experimental and theoretical results:

- The tendon profile did not have a noticeable effect on the deflection of the unbonded prestressed beam. The eccentricity at the interior support reduced the number of cracks at the external load-induced tension zone (top) at the interior support, affected by the effect of the hyperstatic action, which increased the positive moment at that location.

- Because the maximum positive moment developed at the first point load from the external support for the north and south spans and the maximum negative moment occurred at the interior support, the reinforcing bars at the interior support yielded first and the steel bars at the point where the first load was applied yielded at a comparable loading state. In both spans, the steel bars at the second point load from the external support did not yield. Moreover, the steel bars at the bottom of the interior support did not reach the compressive yielding point, which indicated that the prestressing did not have a noticeable effect at the compression zone (bottom) of the interior support. The moment in concrete from the equivalent load replacing tendons resulted in an increase in the compression stress at the top of TB2a and TB2b at the interior support, where no cracks developed on either the top or bottom concrete surface at that location prior to loading.

- Because of the difference between TB1 and TB2a in terms of the distance from the extreme compression fiber to the centroid of the steel strands at the interior support, the slopes of the applied load–strand tension relationship for the two specimens also differed. Specifically, the slope of the strain–applied load tension relationship for TB2a, which had a larger tendon profile depth, was greater than that for TB1.

- During loading, cracks occurred at the tension face of the interior support and then cracking began in the midspan in both the north and south spans. Uniformly distributed cracks were observed at the interior support from both sides. Because the positive hyperstatic moment at the interior support was greater for TB1 than for TB2a and TB2b, the negative moment at the same support was less in TB1 than in the other two specimens. As a result, TB1 had fewer cracks than TB2a and TB2b. In contrast, the cracks at the midspan of the north and south spans for all specimens were distributed from the first point load to the midspan because of the maximum positive moment occurring at the zone.

- The interior support was a roller condition with no vertical restraint, and common statics suggest that

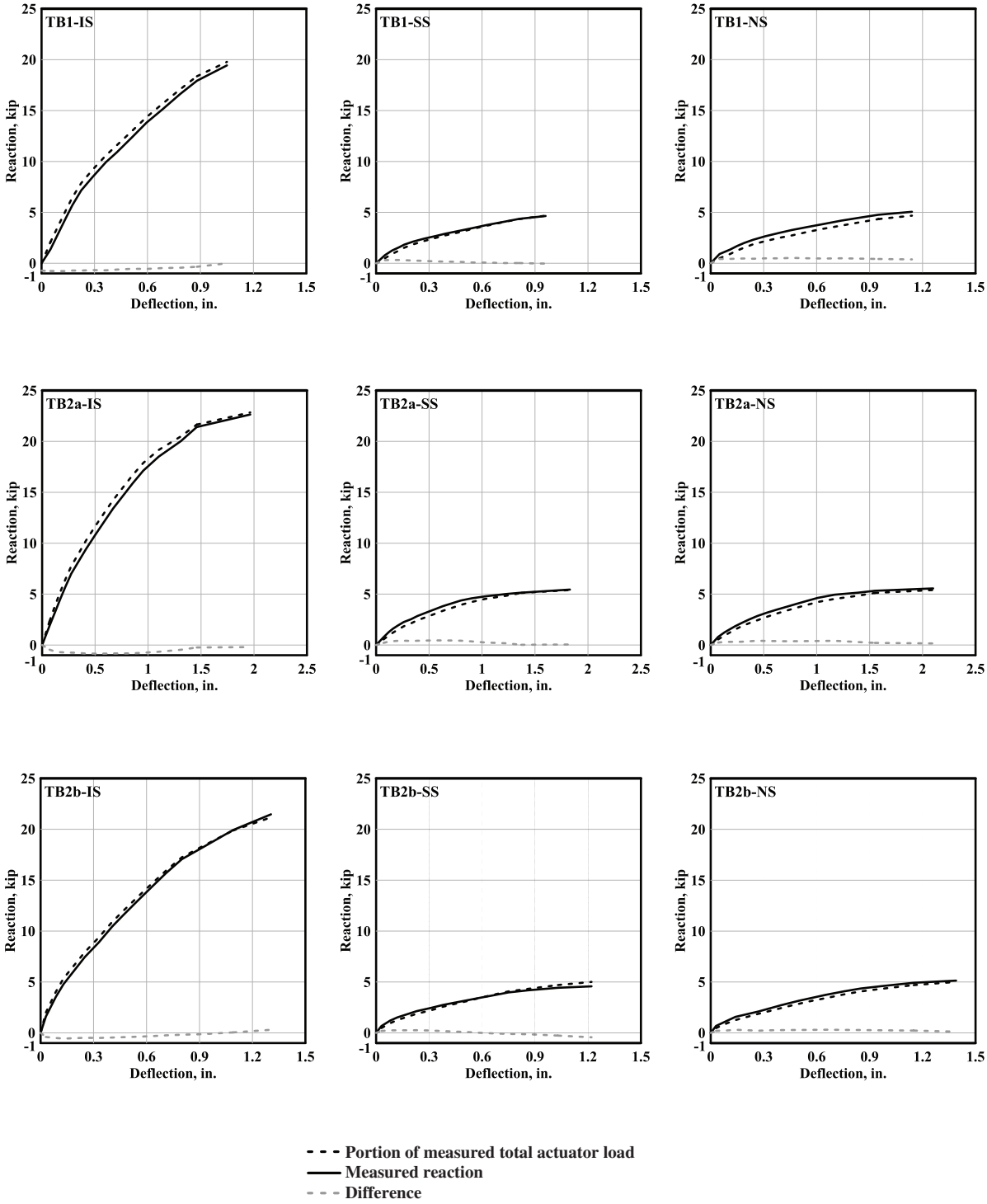

Figure 12. Deflection versus support reaction curves for all three specimens. Note: TB1-IS = T beam specimen 1 at interior support; TB1-NS = T beam specimen 1 at north support; TB1-SS = T beam specimen 1 at south support; TB2a-IS = T beam specimen 2a at interior support; TB2a-NS = T beam specimen 2a at north support; TB2a-SS = T beam specimen 2a at south support; TB2b-IS = T beam specimen 2b at interior support; TB2b-NS = T beam specimen 2b at north support; TB2b-SS = T beam specimen 2b at south support. 1 in. = 25.4 mm; 1 kip = 4.448 kN.

hyperstatic moment would therefore not occur at the interior support. However, differences between the theoretical and experimental reaction values were observed at the interior support after prestressing. The observed behavior indicates that hyperstatic moment occurred at the interior support due to the cold welding effect and partial restraint existed. For all three specimens, hyperstatic reaction then decreased as loading increased and this reaction eventually approached zero, which may imply that the contact welding almost disappeared. Based on the current study only, the effect of hyperstatic moment may need to be included in the calculation of concrete stresses at the service level, but it may not need to be included in the process of ultimate strength design for beams with vertically unconfined supports. That is, the balancing moment M_b consisting of primary and (secondary) hyperstatic moment ($M_1 + M_2$) should be accounted for during the allowable stress design. Additional research for continuous prestressed concrete beams would be necessary to test this hypothesis.

Acknowledgments

The work presented in this paper was funded by California State University, Fullerton, and the Korea Foundation of Nuclear Safety (grant 2003007-0120-CG100). The views expressed are those of authors and do not necessarily represent those of the sponsors.

References

1. Tadros, M. K., N. Al-Omaishi, S. J. Seguirant, and J. G. Gall. 2003. *Prestress Losses in Pretensioned High-Strength Concrete Bridge Girders*. NCHRP (National Cooperative Highway Research Program) report 496. Washington, DC: Transportation Research Board. https://onlinepubs.trb.org/onlinepubs/nchrp/nchrp_rpt_496.pdf.

2. Kang, T. H.-K., and M. Ibrahim Ary. 2012, "Shear-Strengthening of Reinforced and Prestressed Concrete Beams Using FRP: Part II—Experimental Investigation." *International Journal of Concrete Structures and Materials* 6: 49–57. https://doi.org/10.1007/s40069-012-0005-0.

3. Lin, T. Y., and K. Thornton. 1972. "Secondary Moment and Moment Redistribution in Continuous Prestressed Concrete Beams." *PCI Journal* 17 (1): 8–20. https://doi.org/10.15554/pcij.01011972.8.20.

4. Kim, K., and T. H.-K. Kang. 2019. "Experiments on Continuous Unbonded Post-Tensioned Beams with 2,400 MPa (350 ksi) Strands." *ACI Structural Journal* 116 (5): 125–136.

5. Aalami, B. O. 1990. "Load Balancing: A Comprehensive Solution to Post-Tensioning. *ACI Structural Journal* 87 (6): 662–670.

6. Alkhairi, F. M., and A. E. Naaman. 1993. "Analysis of Beams Prestressed with Unbonded Internal or External Tendons." *Journal of Structural Engineering* 119 (9): 2680–2700.

7. Cohn, M. Z., and Z. Lounis. 1993. "Optimum Limit Design of Continuous Prestressed Concrete Beams." *Journal of Structural Engineering* 119 (12): 3551–3570.

8. Kodur, V. K. P., and T. I. Campbell. 1997. "Evaluation of Moment Redistribution in a Two-Span Continuous Prestressed Concrete Beam." *ACI Structural Journal* 93 (6): 721–728.

9. Lopes, S. M. R., J. Harrop, and A. E. Gamble. 1997. "Study of Moment Redistribution in Prestressed Concrete Beams." *Journal of Structural Engineering* 123 (5): 561–566.

10. Barr, P. J., B. M. Kukay, and M. W. Halling. 2008. "Comparison of Prestress Losses for a Prestress Concrete Bridge Made with High-Performance Concrete." *Journal of Bridge Engineering* 13 (5): 468–475. https://doi.org/10.1061/(ASCE)1084-0702(2008)13:5(468).

11. Ayoub, A., and F. C. Filippou. 2010. "Finite-Element Model for Pretensioned Prestressed Concrete Girders." *Journal of Structural Engineering* 136 (4): 401–409.

12. Nie, J., M. Tao, C. S. Cai, and S. Li. 2011. "Analytical and Numerical Modeling of Prestressed Continuous Steel-Concrete Composite Beams." *Journal of Structural Engineering* 137 (12): 1405–1418.

13. Zhou, W., and W. Z. Zheng. 2010. "Experimental Research on Plastic Design Method and Moment Redistribution in Continuous Concrete Beams Prestressed with Unbonded Tendons." *Magazine of Concrete Research* 62 (1): 51–64.

14. Lou, T., S. M. R. Lopes, and A. V. Lopes. 2013. "Flexural Response of Continuous Concrete Beams Prestressed with External Tendons." *Journal of Bridge Engineering* 18 (6): 525–537.

15. Lou, T., S. M. R. Lopes, and A. V. Lopes. 2014. "External CFRP Tendon Members: Secondary Reactions and Moment Redistribution." *Composites: Part B* 57: 250–261.

16. Witchukreangkrai, E., H. Mutsuyoshi, and T. Aravinthan. 2003. "Secondary Moment and Moment Redistribution in a Two-Span Continuous PC beam with Large Eccentricity." *Japanese Concrete Institution* 25 (2): 775–780.

17. Aravinthan, T., E. Witchukreangkrai, and H. Mutsuyoshi. 2005. "Flexural Behavior of Two-Span Continuous Prestressed Concrete Girders with Highly Eccentric External Tendons." *ACI Structural Journal* 102 (3): 402–411.

18. ASTM International. 2016. *Standard Specification for Deformed and Plain Carbon-Steel Bars for Concrete Reinforcement*. ASTM A615/A615M-16. West Conshohocken, PA: ASTM International. https://doi.org/10.1520/A0615_A0615M-16.

19. ACI (American Concrete Institute) Committee 318. 2019. *Building Code Requirement for Structural Concrete (ACI 318-19) and Commentary (ACI 318R-19)*. Farmington Hills, MI: ACI.

Notation

A_{ps} = area of prestressing longitudinal tension reinforcement

b = width of compression face of member

d_p = distance from extreme compression fiber to centroid of prestressing reinforcement

f'_c = specified compressive strength of concrete

f_{ps} = stress in unbonded prestressing reinforcement

f_{pu} = specified tensile strength of prestressing reinforcement

f_{py} = specified yield strength of prestressing reinforcement

f_{se} = effective prestress

F = prestressing force

F_u = ultimate tensile strength of bonded reinforcement

F_y = yield strength of bonded reinforcement

h = height of member

H_1 = equivalent concentrated load calculated by θ_1

H_2 = equivalent concentrated load calculated by $2\theta_1$

H_3 = equivalent concentrated load calculated by θ_2

H_4 = equivalent concentrated load calculated by θ_3

l_n = length of clear span measured from face to face of supports

L_1 = distance between the end support and the concentrated loading point

L_2 = distance between two concentrated loading points in a span

M_b = balancing moment

M_{bB} = balancing moment at point B

M_{bD} = balancing moment at point D

M_{bE} = balancing moment at point E

M_1 = primary moment

M_{1B} = primary moment at point B

M_{1d} = primary moment at point D

M_2 = hyperstatic moment

M_{2B} = hyperstatic moment at point B

P = vertical load

δ = distance between the center of gravity of concrete and the lowest sag point of tendon profile

δ_1 = distance between the center of gravity of concrete and the highest point of tendon profile at center

θ_1 = angle of the profile at H_1

θ_2 = angle of the profile at H_3

θ_3 = angle of the profile at H_4

ρ_p = ratio of A_{ps} to bd_p

About the authors

Uksun Kim, PhD, PE, is a professor in the Department of Civil and Environmental Engineering at California State University, Fullerton.

Ehab N. Ballu is a former master's student in the Department of Civil and Environmental Engineering at California State University, Fullerton.

Seongwon Hong, PhD, is an associate professor in the Department of Safety Engineering at Korea National University of Transportation and was a postdoctoral researcher in the Engineering Research Institute at Seoul National University.

Thomas H.-K. Kang, PhD, PE, is a professor in the Department of Architecture and Architectural Engineering and the Engineering Research Institute at Seoul National University.

Abstract

Approximately half-scale tests were conducted to investigate the behavior of indeterminate prestressed concrete T beams with two different unbonded tendon profiles. Three T beams were employed for the tests: T beam specimen 1 (TB1) was the control specimen and had no eccentricity at the interior support and T beam specimens 2a and 2b (TB2a and TB2b) had eccentricity at the interior support. The results indicate that the specimens with eccentricity at the interior support had a greater number of cracks than the control specimen at the tension zone of the support. This finding was explained by hyperstatic moment reducing the negative moment in the control. The trend in the slope of the strain-applied load tension relationship was different in TB1 than in TB2a due to a difference between the specimens in terms of the distance from the extreme compression fiber to the centroid of reinforcement at the support. Although the interior support was a roller with no vertical restraint, hyperstatic moment at the support occurred due to a cold welding effect, creating a partial roller condition. The hyperstatic action then decreased as the loading was increased. In light of this, the authors conclude that the effect of hyperstatic moment should be accounted for in the calculation of concrete stress at the service level for continuous prestressed concrete beams with unbonded tendons and a vertically unconfined support condition.

Keywords

Continuous beam, intermediate prestressed concrete beam, hyperstatic action, support condition, T beam, unbonded tendon.

Review policy

This paper was reviewed in accordance with the Precast/Prestressed Concrete Institute's peer-review process. The Precast/Prestressed Concrete Institute is not responsible for statements made by authors of papers in *PCI Journal*. No payment is offered.

Publishing details

This paper appears in *PCI Journal* (ISSN 0887-9672) V. 67, No. 4, July–August 2022, and can be found at https://doi.org/10.15554/pcij67.4-01. *PCI Journal* is published bimonthly by the Precast/Prestressed Concrete Institute, 8770 W. Bryn Mawr Ave., Suite 1150, Chicago, IL 60631.

Reader comments

Please address any reader comments to *PCI Journal* editor-in-chief Tom Klemens at tklemens@pci.org or Precast/Prestressed Concrete Institute, c/o PCI Journal, 8770 W. Bryn Mawr Ave., Suite 1150, Chicago, IL 60631.